Collision Cross Sections, Pressure-Broadening Coefficients and Second Virial Coefficients for the Acetylene-Argon Complex: Experiments and Calculations on a New Potential Energy Surface

David Cappelletti*

Dipartimento di Ingegneria Civile ed Ambientale, Università di Perugia, Perugia, Italy

Massimiliano Bartolomei, Marta Sabido,† and Fernando Pirani

Dipartimento di Chimica, Università di Perugia, Perugia, Italy

Ghislain Blanquet and Jacques Walrand

Laboratoire de Spectroscopie Moléculaire, Facultés Universitaires Notre-Dame de la Paix, B-5000 Namur, Belgium

Jean-Pierre Bouanich

Laboratoire de Photophysique Moléculaire (CNRS), Université de Paris Sud, Bât. 350, Campus d'Orsay, F-91405 Orsay Cedex, France

Franck Thibault

Laboratoire de Physique des Atomes Lasers Molécules et Surfaces (UMR-CNRS 6627), Université de Rennes I, Campus de Beaulieu, F-35042 Rennes Cedex, France

Received: March 15, 2005; In Final Form: May 16, 2005

Integral cross sections and pressure-broadening coefficients have been measured by molecular beam scattering and by high-resolution infrared spectroscopy, respectively, for the acetylene−argon system. A new potential energy surface (PES) is proposed to describe structure and dynamical properties of this prototypical weakly bound complex. The PES has been parametrized exploiting a novel atom-bond pairwise additive scheme and has been fitted to the experimental data. Calculations of the scattering cross sections (both differential and integral), pressure-broadening, and second virial coefficients have been performed using both the present and also the most recent ab initio PES available in the literature. Analysis of the new experimental data indicates that the anisotropy of the interaction in the well region should be larger than that obtained in ab initio calculations. This is also in line with previous spectroscopic results.

1. Introduction

Weakly bound complexes involving acetylene, a nonpolar linear molecule, have received much attention in recent years because of their peculiar intermolecular potential mainly affected by the features of the triple bond of acetylene. Further interest stems from the need to help observation and modeling the role of acetylene in planetary and Earth atmospheres. Acetylene is a trace constituent of the Earth's atmosphere mainly produced by anthropogenic sources.[1] It has also been detected in the atmosphere of Jupiter, Saturn,[2] and Titan.[3] These traces are essentially produced by photodissociation of methane,[4] and thus, its concentration in our atmosphere should substantially increase soon. For these atmospheric applications, a detailed knowledge of collisional line broadening is required. More generally, line profile studies can improve our knowledge about intermolecular interactions and associated processes of collisional perturbation of molecular motion. Pressure-broadening effects are closely related to the total population transfer rate among rovibrational states and thus may provide information on molecular relaxation processes. The measure of pressure-broadening coefficients may be useful to test the accuracy of a potential energy surface (PES), especially if experimental values are available over a wide range of temperatures, as shown recently for instance in refs 5, 6. The Ar broadening of few IR lines of the ν_5 band of C_2H_2 have been reported by Varanasi[7] at room and low temperatures; Pine[8] has also measured *R* and *Q* lines in the $\nu_1 + \nu_5$ band in order to study line-mixing effects in the *Q* branch. Valipour et al.[9] investigated the rotational state dependence of the broadening in the $\nu_1 + 3\nu_3$ combination band, as induced by various gases at room temperature. More recently,[10] pressure-broadening coefficients were measured in the *R* and *P* branch of the ν_5 band at 297 K and for some *R* lines at 173 K.

Among the various complexes of acetylene, Ar−C_2H_2 has been the subject of several spectroscopic studies. DeLeon and Muenter[11] first identified this complex by molecular beam electric resonance spectroscopy and proposed a T-shaped equilibrium structure with C_{2v} symmetry. Their analysis gave an argon−acetylene center-of-mass distance of 3.20 Å. Subsequently, Ohshima et al.,[12] by using Fourier transform microwave

* Corresponding author. E-mail: david.cappelletti@unipg.it.
† Present address: University of Barcelona, Spain.

10.1021/jp051347x CCC: $30.25
Published on Web 09/02/2005

spectroscopy, determined a larger equilibrium distance (4.04 Å). Infrared laser spectroscopy was carried out by Hu et al.[13] and Bemish et al.[14] Overall, these investigations suggested a nonrigid T-shaped geometry with a large amplitude in-plane bending modes. The "floppiness" of this complex has hampered deduction of precise structural parameters.

The first empirical potential energy surface for the $Ar-C_2H_2$ system was in fact constructed by Hutson and Thornley[15] in 1992 (A-500 in the following) using a model based on atom−atom pairwise additivity, with parameters chosen to reproduce the rotational transitions observed in the microwave experiment.[12] Bemish et al.[14] constructed a Hartree−Fock plus damped dispersion PES by combining the results of an ab initio calculation at short range with a long-range distributed dispersion interaction. Their rotationally resolved infrared spectroscopic data was used to adjust the parameters.

Besides the spectroscopic surveys, a collisional study of this complex, on the basis of the measure of total differential cross sections (DCS),[16] has been done. In this investigation, Yang and Watts measured well-resolved and moderately damped rainbow oscillations that permitted obtaining both an effective isotropic potential curve and an empirical potential energy surface. An improved version of such a PES (MB in the following), also based on a partial analysis of spectroscopic data, was later presented by the same authors.[17]

Ab initio calculations of the PES at the MP2 level have been presented by Bone[18] in 1994, who deduced a value for the equilibrium separation of 3.8−3.9 Å. Later on, Tao et al.[19] calculated a new PES at the MP4 level with an extended basis set. Rotational constants were found in good agreement with some of the experimentally extracted values; however, the comparison with DCS results indicated a too-shallow potential well. More recently, Yang et al.[20] provided new extensive ab initio calculations of the interaction energy up to the CCSD(T) level. These ab initio PESs were modified by scaling the correlation energy with a geometry-independent factor, optimized by comparing the results of close-coupling calculations with DCS and spectroscopic data. The best of the PESs proposed in this work, denoted CCSD130 and considered in the following discussion, reproduces well the DCS data and also gives a qualitative agreement with the spectroscopic data, even though it is still not satisfactory at a quantitative level. The need for an improvement was explicitly prompted by these researchers who requested in particular new experimental information.

The present work reports new sets of scattering data and pressure-broadening coefficients on the acetylene−argon system. In particular, integral scattering cross sections (ICS) as a function of the collision energy have been measured for the first time. The collisional experiment has been carried out using acetylene molecular beams scattered on argon atom targets kept in a scattering cell. This technique has been applied in Perugia for more than two decades for the characterization of intermolecular forces, the most recent examples being for atom−atom,[21] for atom−molecule,[22,23] and for molecule−molecule systems.[24] Furthermore, the integral cross section is one of the few measurable quantities that are sensitive to the absolute scale and intermolecular range of the interaction energy. To analyze the ICS data, a potential energy surface has been generated, exploiting a novel atom-bond parametrization of the interaction energy.[25] All the interaction potential parameters have been anticipated by semiempirical calculations;[26,27] during the analysis, some of them have been taken as fixed and a few others have been fine-tuned by fitting the experimental integral cross sections. A comparison with calculations performed using the CCSD130 PES[20] will be presented. Differential cross sections have been also computed in order to make a more exhaustive analysis of the scattering results.

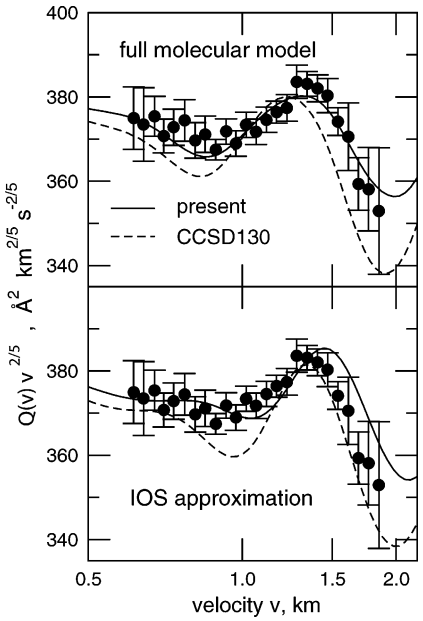

Figure 1. Experimental total cross sections $Q(v)$ for scattering of rotationally "hot" acetylene near effusive beams by argon, plotted as $Q(v) \times v^{-2/5}$, as a function of the beam velocity v. Continuous and dashed lines are calculations with the present and the CCSD130[20] PESs. Upper panel: calculations performed within the full molecular model (see text). Lower panel: calculations performed with an IOS approximation.

Pressure-broadening (PB) calculations are performed with this new PES and with the CCSD130 PES. These values are compared with the measurements that have been carried out in Namur[10] and which are extended in the present work in the *R* branch and provide additional data in the *P* branch at the lowest temperature investigated (173 K). These data are strongly affected by the anisotropy of the interaction. We will show that the simultaneous analysis of ICS, PB coefficients, and DCS provide valuable new information on the PES of the argon−acetylene complex.

Finally, we use the new obtained PES to provide calculations of the second virial coefficients. Up-to-date experimental information on the second virial coefficients is not available.

Details of the experiments are summarized in the next section. Section 3 will present the representation of the PES. Section 4 will outline the data analysis, while a discussion and some final remarks will follow in Sections 5 and 6.

2. Experimental Section

2.1. Integral Cross Sections. The molecular beam apparatus employed for scattering cross sections measurements has been described in detail elsewhere.[22,23] Total (elastic plus inelastic) integral cross sections $Q(v)$ have been measured in the velocity range $0.6 \leq v \leq 2.2$ km/s. The experimental values of $Q(v)$ are reported in Figure 1 as a function of the acetylene beam velocity, v, and have been plotted as $Q(v) \times v^{2/5}$ as usual to emphasize the glory structure.

Two different types of cross section measurements have been carried out. The first experiment has been performed by using effusive beams containing rotationally "hot" acetylene molecules scattered by argon atoms confined in a scattering chamber. The acetylene beam has been produced by expanding the gas, kept at a stagnation pressure of few mbars, through a 1-mm nozzle.

TABLE 1: Ar-Broadening Coefficients γ_0 (in 10^{-3} cm^{-1} atm^{-1}) in the *P* and *R* branches of the ν_5 Band of C_2H_2 at 173.2 K[a]

	P Branch				*R* branch			
m	VP	RP[b]	RP[c]	SDRP[c]	VP	RP[b]	RP[c]	SDRP[c]
2					116.7 (3.5)	117.6 (3.5)	117.0 (3.5)	120.0 (3.6)
3	115.0 (2.8)	116.5 (3.0)	115.5 (2.6)	118.6 (2.6)	108.6 (3.4)	111.1 (4.3)	109.3 (3.4)	112.4 (3.5)
4	107.0 (3.4)	109.9 (3.7)	108.7 (3.2)	111.5 (3.3)				
5					99.6 (2.6)	102.6 (2.5)	100.6 (2.7)	103.3 (2.9)
6	96.4 (2.4)	99.6 (3.1)	97.4 (2.8)	100.0 (3.0)	96.0 (2.0)	97.0 (2.5)	96.4 (2.1)	98.7 (2.1)
7	92.5 (2.1)	93.7 (2.4)	93.0 (2.0)	95.0 (2.0)				
8					87.1 (2.5)	89.4 (3.4)	88.3 (2.3)	90.5 (2.5)
9	87.3 (3.3)	89.4 (2.7)	88.1 (3.1)	90.1 (3.2)				
11					82.5 (1.9)	85.1 (2.5)	83.6 (2.0)	85.8 (2.1)
12					82.6 (2.2)	83.9 (2.1)	83.2 (2.1)	85.2 (2.2)
13	82.8 (2.2)	84.4 (2.8)	83.4 (2.2)	85.2 (2.3)				
15	80.2 (1.8)	82.2 (2.7)	81.1 (2.0)	83.0 (2.3)				
16	76.1 (2.3)	75.9 (2.7)	77.2 (2.2)	79.0 (2.4)				
17					72.1 (1.9)	72.5 (2.8)	74.2 (2.3)	76.3 (2.6)
18	71.4 (2.2)	73.4 (2.4)	72.2 (2.0)	73.9 (2.1)				
19					70.0 (2.0)	71.3 (2.9)	70.8 (2.4)	72.4 (2.6)
22					62.6 (1.9)	65.6 (1.7)	64.1 (1.6)	65.5 (1.7)
25					55.1 (1.6)	56.9 (2.1)	57.0 (1.6)	58.4 (1.9)
28					44.3 (2.0)	49.7 (2.5)	47.3 (2.3)	48.7 (2.5)

[a] Experimental uncertainties are reported in brackets. Note: The experimental results are derived from the fits of the Voigt profile (VP), the Rautian profile (RP) with successively the parameter β_c fitted[b] and fixed,[c] and the speed-dependent Rautian profile (SDRP) with fixed[c] β_c and q parameters. The results for *R*-lines with $|m| = 2,3,6,11,12,17,22$, and 28 have been obtained previously.[10]

The source has been heated at $T \sim 500$ K in order to boost the rotational temperature of the acetylene molecules, which can be assumed to coincide with the nozzle temperature because no relaxation is expected under the present effusive expansion conditions. The molecular beam, velocity selected by a mechanical velocity selector (full width at half-maximum $\sim 5\%$), passes the scattering chamber and is monitored by a quadrupole mass spectrometer. The target gas, Ar in this case, has been maintained at a temperature of 90 K in order to reduce the blurring of possible quantum oscillations in the cross sections due to its thermal motion. As we will see, the observation of a well-developed quantum interference "glory" pattern has been crucial to test the reliability of the intermolecular potential and the dynamics used to describe the acetylene−rare gas collisions (see below). As done previously,[21,22,24] the absolute values of total cross sections have been obtained by an internal calibration on the basis of direct measurements of the gas flowing in the scattering chamber and on the absolute value of He−Ar elastic scattering cross section reported in ref 28.

The second type of measurements has involved the scattering of seeded supersonic beams containing rotationally "cold" and aligned acetylene molecules on argon atoms. These results are a probe both of collisional alignment in the molecular beam[29] and of the PES driving the collisions. As a consequence, they will be not included in the present analysis. On the other side, the present PES has been already used for a quantitative assessment of the degree of collisional alignement in the molecular beam.[30] The details of the latter experiments will be reported elsewhere.

2.2. Pressure-Broadening Coefficients. In this paper, we have extended to a larger number of lines previous measurements at low temperatures, carried out in Namur,[10] for Ar-broadening coefficients in the ν_5 band of C_2H_2. The spectra were recorded with an improved Laser Analytics tunable diode laser spectrometer described in detail elsewhere,[31] equipped with a low-temperature cell. To increase the signal-to-noise ratio, each record was averaged over 100 scans with a sweep frequency of 13.5 Hz. The acetylene sample was provided by Air Products with a stated purity of 99.6% and argon by L'Air Liquide with a stated purity of 99.99%. The absorption cell, with an optical path length of 40.43 cm similar to that described previously,[32] was cooled, and the temperature of the gas was kept constant at 173.2 K ± 0.5 K. For each broadened line, we have recorded four spectra with a constant partial pressure of C_2H_2, while the pressure of Ar was varying from 30 to 70 mbar. Depending on the line under study, the partial pressure of C_2H_2 was ranging from 0.022 to 1.17 mbar. The pressures were measured with two MKS Baratron gauges with a full-scale reading of 1.2 and 120 mbar. The study of an absorption line of C_2H_2 perturbed by Ar required eight consecutive spectra: records of the empty cell, the four broadened lines, the étalon fringes, the pure C_2H_2 line at very low pressure (≤ 0.01 mbar), providing an effective Doppler profile, and a saturated spectrum of this line, giving the 0% transmission level. The assignments and wavenumbers of the measured lines of C_2H_2 in the ν_5 band are taken from ref 33. After being recorded, the nonlinear tuning of the diode laser radiation was corrected with a constant step of about $1\ 10^{-4}$ cm^{-1} by using the étalon fringe pattern.

The data reduction procedure has been thoroughly described elsewhere[10] and will not be repeated in detail here. The collisional half width at half-maximum (HWHM) γ_c have been obtained by fitting the individual profile of each line to Voigt (VP), Rautian[34] (RP), and speed-dependent Rautian models[35] (SDRP). The normalized, per argon atmosphere, broadening coefficients γ_0 are successively obtained by least-squares fitting of the pressure dependence of the collisional half widths. These coefficients measured at 173.2 K in ref 10 and in the present study are presented in Table 1 for the different profiles used, along with the experimental errors. The main sources of uncertainties in the γ_0 values arise from the baseline location, the perturbation due to nearby interfering lines, the nonlinear tuning of the laser, and the line shape model used. The absolute errors that do not account for the uncertainties due to the line shape model are estimated to be equal to the statistical error on γ_0 derived from the linear least-squares fit plus 2% of γ_0. The linearity of γ_c with pressure, and consequently our estimated uncertainties, obtained from the Rautian profiles that closely fit the spectral data, is not better than that derived from the Voigt profile. Within these uncertainties, the broadening coefficients are only $|m|$ dependent [$m = -j$ for $P(j)$ lines and $m = j + 1$ for $R(j)$ lines]. The coefficients derived from the SDRP are significantly larger than those derived from the VP

TABLE 2: Potential Parameters for the CC Triple Bond (CC_{tr}), and CH−Ar Pairs[a]

pair	$R_{m\perp}$	$R_{m\|\|}$	$\epsilon_\perp$	$\epsilon_{\|\|}$
CC_{tr}−Ar	3.96	4.20	9.80	10.4
CH−Ar[b]	3.641	3.851	4.814	3.981

[a] The perpendicular and parallel component of R_m and ϵ are in Å and in meV, respectively. [b] The same values as in ref 25.

(average difference 3.6%); the results derived from the other Rautian profiles are generally ranged between the former results.

3. Potential Energy Surface Representation

The analytical representation chosen for the potential energy surface is of the atom-bond pairwise additive type, as recently introduced by some of the authors.[25] Specifically, the interaction energy of the argon−acetylene complex has been represented as the sum of 3 atom-bond interaction terms of the type

$$V(r,\alpha) = \epsilon(\alpha)\left[\frac{6}{n(r,\alpha)-6}\left(\frac{r_m(\alpha)}{r}\right)^{n(r,\alpha)} - \frac{n(r,\alpha)}{n(r,\alpha)-6}\left(\frac{r_m(\alpha)}{r}\right)^6\right] \quad (1)$$

In eq 1, r is the distance of the argon atom from the bond center and α is the angle that **r** forms with the bond considered; ϵ and r_m are, respectively, the atom-bond interaction well depth and its location. The n parameter is expressed as a function of both r and α using the equation:[25]

$$n(r,\alpha) = 9 + 4.0\left(\frac{r}{r_m(\alpha)}\right)^2 \quad (2)$$

The dependence of ϵ and r_m from α is given by the relationships

$$\epsilon(\alpha) = \epsilon_\perp \sin^2(\alpha) + \epsilon_{||} \cos^2(\alpha) \quad (3)$$

$$r_m(\alpha) = r_{m\perp} \sin^2(\alpha) + r_{m||} \cos^2(\alpha) \quad (4)$$

where $\epsilon_\perp$, $\epsilon_{||}$, $r_{m\perp}$, and $r_{m||}$ are, respectively, the well depth and equilibrium distance for the parallel and perpendicular approaches of the Ar atom to the bond. All the parameters necessary to describe the components of the Ar−acetylene interaction are given in Table 2.

This approach treats the interaction as determined by a repulsion due to an effective size of the molecule[26] and an attraction arising from different dispersion centers distributed on the molecule. Such a formulation provides a realistic picture of both the repulsive and the attractive components of the interaction and, in addition, effectively incorporates both three-body[25] and other nonadditive effects. The performances of this parametrization have been recently investigated by calculating static and dynamic properties of atom (and ion) clusters with hydrocarbon molecules.[36]

For the CH bond−Ar interaction, we exploited the same parameters previously used for the description of the CH_4−Ar and C_6H_6−Ar complexes.[25] The CH bonds here are assumed to have electronic charge distributions of near-cylindrical symmetry. In each atom-bond pair, the reference point is set to coincide with the geometric bond center because the dispersion center and the bond center coincide for the CC triple bond and are almost coincident for CH.

Values for the CC triple bond−Ar term are given here and have been evaluated by using a semiempirical method,[27] employing as input data the CC triple bond polarizability tensor components and the Ar atomic polarizability. These initial values have been refined during the fit of the experimental data by varying them within the known uncertainties.

4. Data Analysis

4.1. Scattering Integral Cross Sections. As it is well established,[37] the integral cross section Q exhibits, as a function of the collision velocity v, an oscillatory behavior (glory effect) overimposed to a monotonic component. Typically, the latter, determined by collisions at large impact parameters probing the long-range part of the interaction, decreases as $v^{-2/5}$ and is mainly responsible for the size of the cross section. The glory undulations arise from the interference between two types of trajectories, both leading to zero deflection: the first type corresponds to trajectories at intermediate impact parameters, for which the attractive and repulsive actions balance; the second type is due to collisions unaffected by the potential. Amplitudes and frequencies of these undulations are connected to features of the potential such as the depth of the well ϵ and its location R_m.[37,38]

Close-coupling calculations of $Q(v)$ for atom−molecule cases are feasible and meaningful[22] when the number of the coupled channels is relatively low. In the present case of experiments with a rotationally hot beam ($T_{rot} \sim 500$ K), this approach would require an excessive computational effort. On the other hand, the fast rotational motion of the acetylene molecules may allow some approximations to be introduced in the theoretical description of the collisions without losing any content of information on the interaction potential.

Such approximations are motivated by: (i) the experimental observation that, in atom−molecule collisions, the glory amplitude is not quenched when the average molecular rotation time is comparable or shorter than the collision time;[39] (ii) the theoretical analysis of the effect of the interaction anisotropy in atom−molecule collisions, which shows its vanishing role with the increase of the rotational temperature of the molecules;[40] (iii) the demonstration, by experiments and close-coupling calculations, that ICS in the glory region are dominated by the elastic component of the scattering because the inelasticity vanishes at intermediate and large impact parameters.[41]

Specifically, the collision dynamics has been modeled according to two different limiting regimes: (i) a spherical model, where a central field scattering is operative, and (ii) a molecular model, where the cross sections are determined by a combination of two partial orientationally averaged contributions. We also performed some calculations within an infinite order sudden approximation (IOSA) scheme. Even if it is well-known that such a scheme typically leads to overestimating the role of the PES anisotropy, these calculations have been carried out to provide further arguments to the discussion.

The (i) and (ii) regimes selectively emerge as a function of the ratio between the rotational time t_{av} ($\sim 4 \times 10^{-13}$ s, at $T_{rot} \sim 500$ K), required to induce an average of the interaction between limiting configurations of the complex and the average collision time t_{coll}, which varies with the beam velocity.[23] The estimated times indicate that, at low collisional velocities, $t_{coll} \gg t_{av}$, rotationally excited acetylene molecules rotate sufficiently fast during a collision to be considered as spherical particles. In such conditions, collisions are mainly elastic and driven by the spherical component of the interaction $\bar{V}(R)$, which can be obtained by spherically averaging the PES over the θ angle,

$$\bar{V}(R) = \int_0^{\pi/2} V(R, \theta) \sin\theta \, d\theta \quad (5)$$

where R is the distance from Ar to the acetylene center of mass, and θ is the relative Jacobi angle. At higher velocities, $t_{coll} \sim t_{av}$ and the "molecular" collisional regime sets in. Here, acetylene tends to reveal its character of a linear molecule, even if a partial orientational averaging is present. In this case, an IOSA is not fully appropriate to describe the dynamics. Therefore, an appropriate dynamical model (a "molecular" model) should be characterized by partial averages over the helicity states, defined by the helicity quantum number M (the projection of the rotational angular momentum **j** along the collisional axes). In such conditions, one can assume that collisions are driven by two effective potentials V_{LH} and V_{HH}, which represent partial averages over the low (LH) and high (HH) helicity states, respectively.

Specifically,

$$V_{LH}(R) = 2\int_0^{\pi/3} V(R, \theta) \sin \theta \, d\theta \tag{6}$$

governs the collisions occurring essentially at small θ angles (which correlate with low helicity states),

while

$$V_{HH}(R) = 2\int_{\pi/3}^{\pi/2} V(R, \theta) \sin \theta \, d\theta \tag{7}$$

controls the collisions basically occurring at large θ angles (which correlate with high helicity states).

These partially averaged interactions satisfy the important condition that the spherical average of the interaction can be obtained by the averaged sum of V_{LH} and V_{HH}:

$$\bar{V}(R) = \frac{V_{LH}(R) + V_{HH}(R)}{2} \tag{8}$$

The present model is formulated in the spirit of the centrifugal sudden (CS) approximation, in the sense that it contains a partial helicity conservation scheme. In this respect, it is a less crude approximation to the dynamics than the standard IOSA, which considers the molecules to be frozen during the scattering and can be used only for rotationally cold beams and hyperthermal collision energies. The improvement obtained in the present treatment has been demonstrated by a comparison with IOSA calculations performed with the two PES and reported in Figure 1 (to be discussed below).

The final calculated total cross sections have been obtained within the spherical model for $v \leq 0.7$ km/s and according to the molecular model for $v \geq 1.3$ km/s. In the latter case, the calculated $Q_{LH}(v)$ and $Q_{HH}(v)$ cross sections, corresponding to the collisions driven, respectively, by $V_{LH}(R)$ and $V_{HH}(R)$ interactions, have been then combined as

$$\frac{Q_{LH}(v) + Q_{HH}(v)}{2} \tag{9}$$

The switch between the (i) and (ii) dynamical regimes at intermediate v has been carried out by a weighted sum (the weights depending on the velocity[23]) of cross sections calculated for the two limiting cases.

The scattering cross sections have been calculated in the center of mass systems. Standard numerical techniques have been used for the phase-shift evaluation.[38] The cross sections have been then convoluted in the laboratory frame and compared with the experimental data. A trial-and-error procedure allowed a fine-tuning of some interaction potential parameters, namely, those related to the CC triple bond−Ar interaction term in the atom-bond pairwise additive representation of the PES. The best-fit final results are shown as continuous lines in the upper panel of Figure 1.

4.2. Pressure-Broadening Cross Sections. The pressure-broadening cross section calculations were performed with MOLSCAT[42] quantum dynamical scattering code in which the impact and binary approximations[43,44,45] are assumed. They were derived from close-coupling calculations of scattering S-matrix elements. The coupled equations were solved by means of the hybrid log derivative-Airy propagator of Alexander and Manolopoulos.[46] The propagation was carried out with the log derivative method from a minimum distance, $R_{min} = 2.1$ Å, to an intermediate distance, $R_{mid} = 15$ Å, and then a switch to the Airy method was done up to a maximum intermolecular distance, $R_{max} = 30$ Å. The interaction potential surfaces were projected over six Legendre polynomials $P_\lambda(\cos \theta)$ through the so-called "vrtp" mechanism as implemented in MOLSCAT[42] code. Recall that, because of homonuclear symmetry of acetylene, only even values of λ are needed. The radial coefficients $V_\lambda(R)$ were obtained by a Gauss−Legendre quadrature over 16 points. Here, only half of these points are really needed. The total angular momentum J, with $\boldsymbol{J} = \mathbf{j} + \mathbf{l}$, was held fixed to a maximum value of 150 to ensure the convergence in partial waves (l). Typically, for a kinetic energy of 263 cm^{-1}, the convergence was reached for $J_{max} = 120$ (105) for the $R(0)$ pressure-broadening cross sections (respectively for the $R(22)$ pressure-broadening cross section). All energetically open rotational levels and at least four closed levels, two with odd and two with even rotational angular j values, are included in the calculations for each total energy. Because we compared our calculations with experimental pressure-broadening coefficients for P or R lines, we had to consider both species (ortho and para) of acetylene simultaneously. However, for some cases, two separate calculations have been performed, one for the ortho states with odd j values, and the other for the para states with even j values; then a postprocessor was used to generate the pressure-broadening cross section from the two resulting S matrixes. This method has the great advantage of substantially speeding up the MOLSCAT[42] computation run because the rotational basis is divided by two. This is possible because ortho and para forms do not interconvert when C_2H_2 is colliding with an atom. The rotational energy levels were generated with a fixed rotational constant ($B = 1.176641$ cm^{-1}), and the same PES was considered in both ground and vibrationally excited states of C_2H_2. Indeed, the different Ar−C_2H_2 PESs considered here do not include any vibrational dependence. Drawing on our experience in pressure-broadening calculations,[6,47,48,49,50] and in particular, for ref 50 Ar−C_2H_2, we did not perform the thermal average over a grid of relative barycentric kinetic energies, but only did the calculations at the kinetic energies $\bar{E}_{kin} = (4/\pi)k_B T/hc$ (i.e., 263 cm^{-1} for $T = 297$ K and 153 cm^{-1} for $T = 173$ K) associated with the mean relative velocity $\bar{v} = (8RT/\pi\mu)^{1/2}$ for a given temperature T. Therefore, for each $R(j)$ line studied at a given temperature, we only performed one (or two) MOLSCAT run(s) at the two total energies equal to the collision energy ($\bar{E}_{kin}$) plus the rotational energy in the initial level and in the final level involved in the radiative transition.[43,44,45] This has been shown to be accurate in refs 47 and 49 for CO_2 and CO in argon and has been checked à posteriori for the present system using our previous work,[50] where we did the thermal average of the pressure-broadening cross sections over a grid of energies (see eq 12 below). We thus expect our results to be accurate to within a few percent. Finally, the pressure-broadening parameters, γ_0 (in 10^{-3} cm^{-1} atm^{-1}), were

TABLE 3: Pressure-Broadening Coefficients γ_0 (in 10^{-3} cm^{-1} atm^{-1}) at 297 K[a]

	calculated values		experimental[c] values	
m	present PES[b]	CCSD130 PES[b]	*R* lines	*P* lines
1	92.1	87.2		
2	83.4	79.5	79.6 (3.3)	85.7 (3.0)
3	76.2	73.8	76.8 (2.5)	78.0 (2.7)
4	71.5	69.5		74.4 (2.4)
5	67.6	65.9	68.4 (1.9)	71.1 (2.3)
6	63.8	62.5	66.1 (2.1)	67.2 (2.0)
7	60.3	58.9		
8	57.1	55.0	59.5 (1.9)	60.6 (2.1)
9	54.9	52.6	58.7 (1.8)	58.6 (1.8)
10	54.2	50.5		
11	54.2	49.5	55.5 (2.6)	59.2 (1.8)
12	53.8		54.4 (2.8)	56.2 (1.9)
13	53.7	49.6		
14	52.2		54.8 (1.8)	53.7 (2.8)
15	51.2	48.3	52.5 (2.1)	54.3 (1.8)
16	50.1			
17	49.0	46.8	50.5 (2.4)	
18	47.7		49.0 (1.8)	
19	46.5	44.9		48.6 (1.4)
20	45.3			
21	44.4	43.0		46.1 (1.0)
22	42.7		44.3 (1.0)	44.8 (2.0)
23	41.4	40.1		43.6 (1.9)

[a] Experimental uncertainties are reported in brackets. [b] Calculations for *R* lines at $E_{kin} = 263$ cm^{-1}. [c] Experimental values[10] (obtained with a Rautian profile).

TABLE 4: Pressure-Broadening Coefficients γ_0 (in 10^{-3} cm^{-1} atm^{-1}) at 173 K[a]

	calculated values		experimental[c] values	
m	present PES[b]	CCSD130 PES[b]	*R* lines	*P* lines
1	139.4	129.0		
2	125.0	118.3	117.6 (3.5)	
3	114.8	111.1	111.1 (4.3)	116.5 (3)
4	106.3	104.6		109.9 (3.7)
5	100.3	96.7	102.6 (2.5)	
6	94.8	90.7	97.0 (2.5)	99.6 (3.1)
7	88.0	87.0		93.7 (2.4)
8	85.2	81.7	89.4 (3.4)	
9	85.5	79.3		89.4 (2.7)
10	85.3	77.9		
11	84.3	79.0	85.1 (2.5)	
12	82.6		83.9 (2.1)	
13	80.7	77.3		84.4 (2.8)
14	78.3			
15	76.4	73.9		82.2 (2.7)
16	73.4			75.9 (2.7)
17	71.6	70.0	72.5 (2.8)	
18	69.3			73.4 (2.4)
19	66.9	65.2	71.3 (2.9)	
20	64.4			
21	61.9	60.8		
22	59.2		65.6 (1.7)	
25	52.7	51.5	56.9 (2.0)	
28	46.1	44.9	48.7 (2.5)	

[a] Experimental uncertainties are reported in brackets. [b] Calculations for *R* lines at $E_{kin} = 153$ cm^{-1}. [c] Experimental values (obtained with a Rautian profile).

obtained from the pressure-broadening cross sections, σ_{PB} (in $Å^2$), through

$$\gamma_0 = 56.6915\sigma_{PB}(\mu T)^{-1/2} \quad (10)$$

where the reduced mass of the system $\mu = 15.7575$ u.

The γ_0 values calculated with the described methodology, using both the present and the CCSD130 PES's, are reported in Tables 3−4 and in Figure 2, for a comparison.

5. Discussion

5.1. Integral Cross Sections. Experimental and calculated scattering integral cross sections are compared in the upper panel of Figure 1. As anticipated before such an analysis, which mainly focuses on the reproduction of the amplitude and position of the glory oscillations, and of the absolute value of the total cross section, is a direct probe of the scale of the interaction and a permitted accurate fine-tuning of the potential parameters of the PES here proposed. In the same panel are also reported (as a dashed line) the cross sections calculated using the CCSD130 PES[20] and the (same) dynamical scheme described in Section 4.1. It could be noticed that the absolute value of the cross sections for the CCSD130 PES is within the experimental uncertainty of the experimental cross section. This is not surprising because the spherical averages of the two PESs are very similar, as can be appreciated in Figure 3.

On the other hand, in a finer analysis, the experimental glory position as well as the glory amplitude are not perfectly reproduced by the CCSD130 PES. In particular, the glory oscillations are too large because of the too-low anisotropy in the well region. As a further test, we report in the lower panel of the same figure calculations performed within the IOS approximation for both the present and the CCSD130 PESs. As stated before, IOS calculations overestimated the glory quenching (measured in the present experimental conditions),

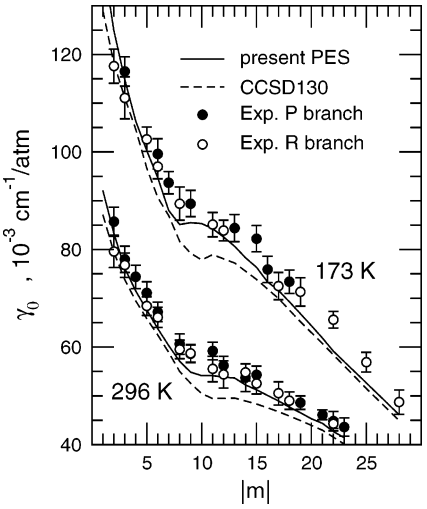

Figure 2. Experimental and calculated pressure-broadening coefficients, γ_0, for the $Ar-C_2H_2$ system, at two different temperatures, for the *P* and *R* branches (full and empty circles, respectively). Calculations have been performed with the present PES and with the CCSD130 PES.[20]

and this is clearly not the case for the CCSD130 PES: this is a manifestation of a too-low interaction anisotropy in the well region.

5.2. Topology of the PES and Comparison with Information from Spectroscopic Studies. The isotropic components of the present and the CCSD130 PES are very similar. A comparison is shown in Figure 3. The curves have been obtained by averaging the corresponding PESs over the angle θ. This is also the reason both PESs reproduce well the DCS data (see below).

A detailed comparison of the anisotropy of the interaction energy is reported in Figures 4−6. In Figure 4, the minimum energy ϵ and the equilibrium distance R_m are plotted as a

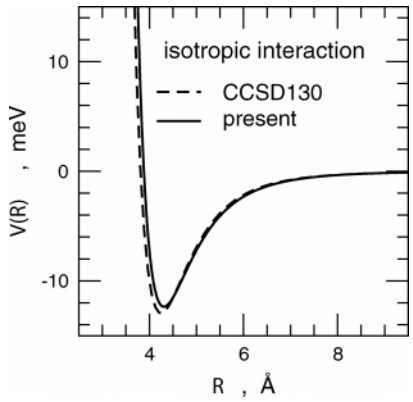

Figure 3. Isotropic component of the interaction energy for the acetylene−Ar system. Comparison between the present and the CCSD130[20] PESs.

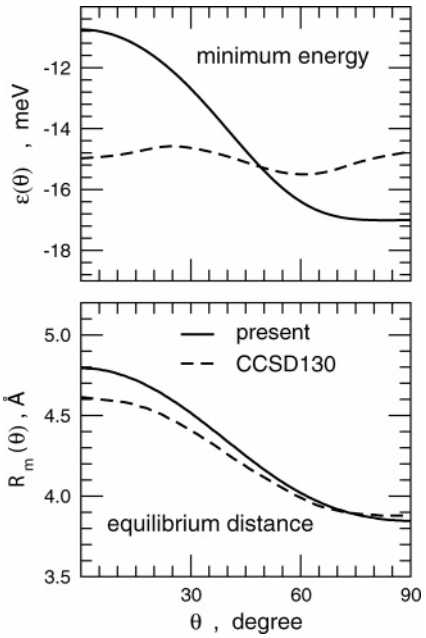

Figure 4. Angular dependence of the minimum energy ϵ and equilibrium distance R_m for the present and the CCSD130[20] PESs.

function of the θ angle. While the two PESs show a similar behavior of R_m, the anisotropy of ϵ is very different and specifically very low for the CCSD130 PES, while it is more marked for the present PES. These differences are also clear from Figure 5, where the two limiting cuts for $\theta = 0$ and 90 degrees are plotted as a function of the intermolecular distance R.

The spectroscopic values for the equilibrium distance are centered around ∼4.0 Å (see for example ref 12), which is consistent with both the present and the CCSD130 PESs (see Figure 4). The ground-state dissociation energy extracted from spectroscopic data is ∼17.8 meV[14], which is also consistent with the present value for the absolute minimum (17 meV), while the CCSD130 PES gives a lower dissociation energy (12.7 meV). We note that the CCSD130 PES underestimates the experimental bending frequency, which indicates a too-low anisotropy in the well region. Also, the simulation of the infrared spectrum made in ref 20 leads the authors to a similar conclusion. Overall, the present PES shows an anisotropy which is between that of the CCSD130 PES (probably too low) and that of the four-center potential of Miller and co-workers,[14] which is believed to give an upper limit. Indeed a critical test

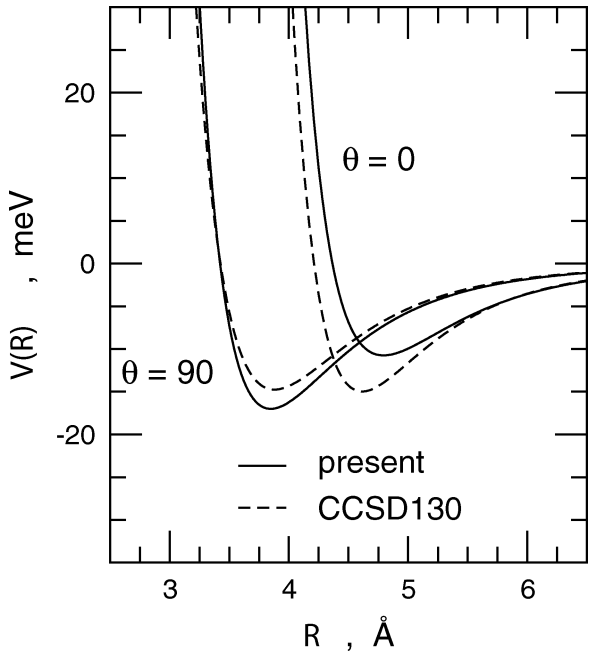

Figure 5. Radial behavior of $\theta = 0$ (collinear) and $\theta = 90$ (T-shaped) geometries of the present and the CCSD130[20] PESs.

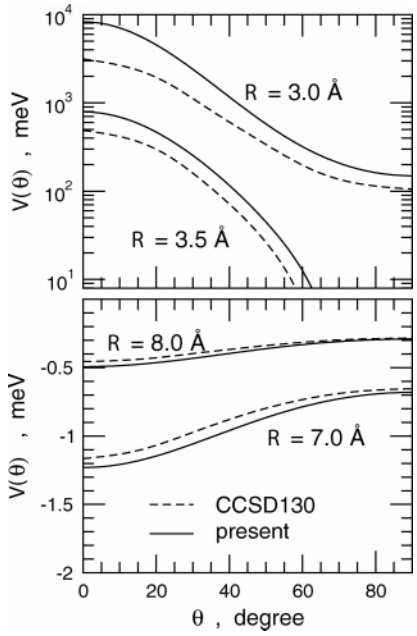

Figure 6. Angular dependence of the potential energy at long range (lower panel) and short range (upper panel) for the present and the CCSD130[20] PESs.

of the present PES should be done by calculating directly the spectroscopic parameters.

Figure 6 reports the behavior of the PESs as a function of the θ angle at long distance (lower panel) and at short range (upper panel). While the two surfaces are quite similar at long range, they are appreciably different in the repulsive region, even if qualitatively they show a similar angular behavior. Near $\theta = 0°$, the present PES is very similar to the MB PES of Yang and Watts,[17] while around the equilibrium T-shaped geometry, it is quite similar to the A-500 PES of Hutson and Thornley,[15] which has been fitted to many spectroscopic data.

5.3. Pressure-Broadening Coefficients. Before comparing the results, it may be interesting to recall some salient features of the pressure broadening. Because a pressure-broadening cross

section is the result of a multitude of collisions with various impact parameters probing both the internuclear separation and the angular dependence of the PES, it is unclear how sensitive the pressure-broadening cross sections are to the details of the PESs. However, because the pressure-broadening cross section are closely related to inelastic integral cross sections $\sigma(j_i \rightarrow j_f; E_{kin})$ (where E_{kin} is the available kinetic energy in the entrance channel j_i), the HWHM of an IR line may be approximated (see refs 6, 47, 49 and references therein) by a sum of rate constants, such as

$$\gamma(j_i, j_f; T) \cong \frac{1}{2}\frac{n_b}{2\pi c}\left(\sum_{i' \neq i} k(j_i \rightarrow j_{i'}; T) + \sum_{f' \neq f} k(j_f \rightarrow j_{f'}; T)\right) \quad (11)$$

where n_b is the density of the gas perturber. The rotational rate constants are in turn related to the thermally average inelastic cross sections $\bar{\sigma}$:

$$k(j_i \rightarrow j_{i'}; T) = \langle v\sigma \rangle \equiv \bar{v}\,\bar{\sigma}(j_i \rightarrow j_{i'}; T) \quad (12)$$

thus, as the anisotropy of a PES increases, the collisional HWHM increases.

Because rate constants of low j values (and especially those with $\Delta j = 1$) are more sensitive to high partial waves, they enable testing of higher internuclear distances than rate constants involving high j values,[5,51] which are more sensitive to lower partial waves (or lower impact parameters). Obviously, this characteristic is tempered by the kinetic energies involved or by the temperatures considered. In fact, it is expected that, for the highest kinetic energies, the dominant interaction arises from the repulsive part of the potentials, while at low energies, say of the order of the minimum, the complete surface should contribute to the broadening rates.[6]

A rough estimate of the regions of a PES probed by a pressure-broadening cross section can be given. From the gas kinetic theory or from the semiclassical models, the pressure-broadening cross section may be written as $\sigma = \pi\tilde{b}^2$ where $\tilde{b}$ is an effective impact parameter. This effective value ranges from 5.9 to 3.95 Å for $j = 0$ to 22 at room temperature.

Experimental and calculated pressure-broadening coefficients at 173 and 297 K are reported in Figure 2 and in Tables 3−4. For the Ar-broadening of acetylene IR lines, it appears that the theoretical results using the PES defined in this work and the CCSD130 PES of Yang et al.[20] are in close agreement. Both PESs reproduce well the magnitude and the behavior of the experimental data. However, some differences exist between the pressure-broadening coefficients derived from both PESs. The values predicted by using the present PES are systematically higher than those arising from the CCSD130 PES;[20] the difference increases for low j values as the temperature decreases. This should be attributed to the larger anisotropy of the present PES, at least around the well (see Figure 4), which gives a better agreement with the experimental values. The CCSD130 PES[20] has been recently used[50] to calculate pressure-broadening coefficients for Raman isotropic Q lines in the ν_2 band. The agreement with the experimental HWHM in the range 134−295 K was rather satisfactory. Thus, it is expected that the present PES should lead to an even better agreement. Indeed, the same differences between both PESs should also manifest for Raman lines (see eq 11, which can be considered as exact for an isotropic Raman line as long as any vibrational dependence is neglected).

The present pressure-broadening coefficients probe the well region of the PESs and also the bottom part of the repulsive wall of the PES, especially when the highest j values are involved at 263 cm^{-1}. Because the present PES is slightly more repulsive and anisotropic in the wall region (see Figures 5 and 6), a better agreement is found with the experimental measurements. However, the repulsive wall is not well tested by our calculations (see above); thus, it would be interesting to have pressure-broadening parameters at higher temperatures (≈1000 K) to better discriminate between both PESs in this region.

Finally, we note that the measured pressure-broadening parameters of Valipour et al.[9] are systematically larger, especially for high j values, than the measured values by Namur's group.[10] This discrepancy can be due either to a systematic bias in the measurements of ref 9 or to a significant vibrational effect because Valipour et al. measured line widths in the $\nu_1 + 3\nu_3$ combination overtone vibrational band involving the C−H stretching. The differences observed between the experimental values of Valipour et al.[9] for R and P lines can only be attributed to experimental uncertainties. In the rigid approximation, we assume the collisional width for a $R(j)$ line is equal to the width of the $P(j + 1)$ line.[45] The experimental values of Bouanich et al.[10] are in line with this assumption. Moreover, these experimental values at room temperature are close to the measurements of Pine[8] in the $\nu_1 + \nu_5$ combination band and to those of Varanasi[7] in the ν_5 band.

5.4. Differential Cross Sections. A further test of the proposed potential energy surface has been carried out, considering the differential cross sections experiment of Yang and Watts[16] on C_2H_2−Ar. These authors measured DCSs in a crossed molecular beam experiment using a moderately supersonic beam of pure acetylene. In such conditions, the molecules are not fully rotationally relaxed, and only some of the lowest rotational states of the molecule contribute to the scattering. As a consequence, the experimental DCSs are only partially damped by the interaction anisotropy. A well-resolved rainbow oscillation was observed, and both effective spherical and anisotropic potentials were obtained from the analysis of the data. The anisotropic potential was obtained using IOS calculations. A full analysis of the DCSs results would require a close-coupling calculation that is beyond the scope of this work as well as the convolution from the center-of-mass to the lab reference systems, which would have required the detailed knowledge of the experimental conditions. We tried here a consistency test, calculating the DCSs for the C_2H_2−Ar system, in the center-of-mass reference frame, with the spherical average $\bar{V}$ of our PES and with the full PES within an IOS scheme. In Figure 7, these cross sections are compared with the ones obtainable from the best-fit effective potential curve reported in ref 16. A good agreement can be observed; in particular, the results from the best-fit potential[16] exhibit, at any angle, a behavior intermediate between the two limiting cases of our calculations. The DCSs calculated with a true spherical potential $\bar{V}$ gives a rainbow peaking at a slightly lower scattering angle than the one obtained from the experimental effective spherical potential, as expected. The IOS calculation with the full PES provides a correct rainbow position, while it overestimates the quenching of the oscillation, which is typical within the IOSA. We can conclude that, within this simple analysis, the present PES is consistent with the DCSs measurements of Yang and Watts.[16]

5.5. Second Virial Coefficients. As an application, we have calculated the second virial coefficients for the Ar−C_2H_2 system using the present PES. Unfortunately, a comparison with experimental values has not been possible because up-to-date values are not available. The results are reported in Table 5

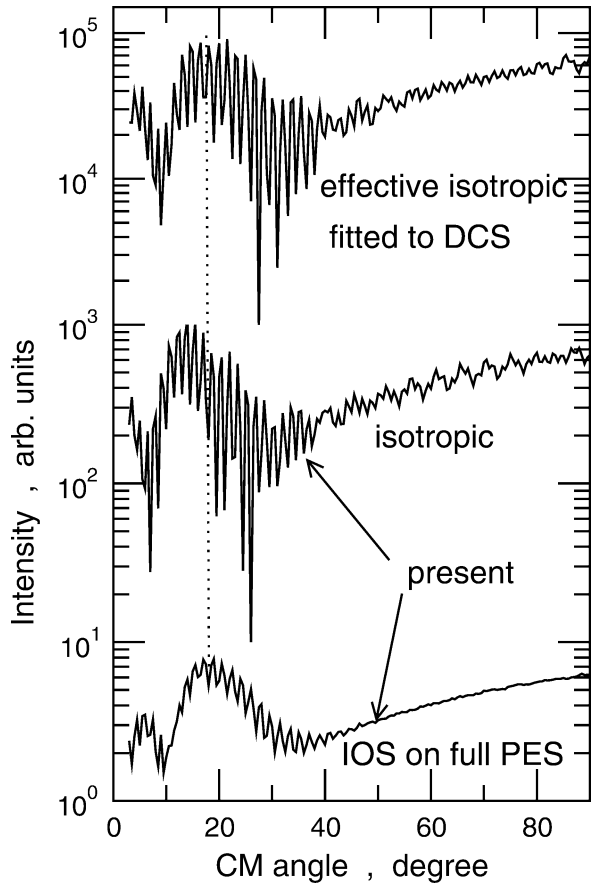

Figure 7. Center of mass calculated differential cross sections for the acetylene−Ar system. At the top are shown results obtained with the effective isotropic potential of ref 16. Result obtained with the spherical average of the present PES and IOS results obtained with the present fully anisotropic PES are also shown (shifted).

TABLE 5: Second Virial Coefficients B (in cm^3 mol^{-1}) as a Function of Temperature, as Calculated with the Present PES[a]

T	B_{clas}	B'_{rad}	B'_{ang}	B'_{cor}	B_{Tot}
90	−439.685	5.005	2.414	0.145	−432.122
100	−355.676	3.488	1.688	0.102	−350.396
110	−295.340	2.565	1.244	0.076	−291.455
125	−231.464	1.743	0.847	0.052	−228.822
140	−186.940	1.265	0.615	0.038	−185.021
150	−164.118	1.051	0.511	0.032	−162.524
170	−129.226	0.763	0.370	0.023	−128.070
190	−103.860	0.583	0.283	0.018	−102.976
220	−76.658	0.418	0.202	0.013	−76.026
240	−63.194	0.346	0.167	0.011	−62.670
250	−57.457	0.318	0.153	0.010	−56.976
300	−35.617	0.221	0.105	0.007	−35.284
350	−21.080	0.165	0.078	0.005	−20.831
400	−10.759	0.130	0.061	0.004	−10.563
450	−3.085	0.106	0.050	0.003	−2.926
473	−0.151	0.097	0.046	0.003	−0.005
500	2.820	0.089	0.042	0.003	2.953
550	7.487	0.076	0.036	0.003	7.601
600	11.254	0.066	0.031	0.002	11.354
700	16.929	0.052	0.024	0.002	17.007
800	20.959	0.043	0.020	0.001	21.023

[a] Classical and first quantum corrections (radial, angular and Coriolis) are reported, as well as the total value B_{Tot}.

and include radial, angular, and Coriolis first quantum corrections.[52] The Boyle temperature of the C_2H_2−Ar system is around 473 K.

6. Conclusions

New experimental results on the argon−acetylene system, specifically integral scattering cross sections and pressure-broadening coefficients, are reported in this work. An extensive analysis of the experimental results, on the basis of accurate dynamical calculations and a model PES, provides fine details on the structure of the complex. In particular, important information has been obtained on the anisotropy and on the absolute depth of the attractive well of the complex. A critical comparison with the most recent and accurate ab initio PES indicates the need to improve the anisotropy component, which seems to be too low, as indicated also by a qualitative comparison with structural parameters coming from spectroscopy. A more stringent test of the accuracy of the present phenomenological PES should be done in the future by directly calculating the spectroscopy of the complex and comparing with the experiments.

Acknowledgment. Part of this work has been carried out under the integrated action GALILEO/GALILEE 2005 between Italy (Perugia) and France (Rennes).

References and Notes

(1) Goldman, J.; Murcray, F. J.; Blactherwhick, R. D.; Gillis, J. R.; Bonomo, F. S. *J. Geophys. Res.* **1981**, *86*, 12143.
(2) Noll, K. S.; Knacke, R. F.; Tokunaga, A. T.; Lacy, J. H.; Beck, S.; Serabyn, E. *Icarus* **1986**, *65*, 257.
(3) Coustenis, A.; Encrenaz, T.; Bezard, B.; Bjoraker, G.; Graner, G.; Dang-Nhu, M.; Arié, E. *Icarus* **1993**, *102*, 240.
(4) Hanel, R.; Conrath, B.; Flasar, M.; Kunde, V. G.; Maguire, W.; Pearl, J.; Pirraglia, J.; Samuelson, R. C.; Herath, L.; Allison, L.; Cruickshank, D.; Gauthier, D.; Gierasch, P.; Horn, L.; Kumar, S.; Ponnamperuma, C. *Science* **1981**, *212*, 192.
(5) Roche, C. F.; Ernesti, A.; Hutson, J. M.; Dickinson, A. S. *J. Chem. Phys.* **1996**, *111*, 2156.
(6) Thibault, F.; Calil, B.; Boissoles, J.; Launay, J.-M. *Phys. Chem. Chem. Phys.* **2000**, *2*, 5404.
(7) Varanasi, P. *J. Quant. Spectrosc. Radiat. Transfer* **1992**, *47*, 263.
(8) Pine, A. S. *J. Quant. Spectrosc. Radiat. Transfer* **1993**, *50*, 149.
(9) Valipour, H.; Zimmermann, D. *J. Chem. Phys.* **2001**, *114*, 3535.
(10) Bouanich, J.-P.; Blanquet, G.; Walrand, J. *J. Mol. Spectrosc.* **2003**, *219*, 98.
(11) DeLeon, R. L.; Muenter, J. S. *J. Chem. Phys.* **1980**, *72*, 6020.
(12) Ohshima, Y.; Iida, M.; Endo, Y. *Chem. Phys. Lett.* **1989**, *161*, 202.
(13) Hu, T. A.; Prichard, D. G.; Sun, L. H.; Muenter, J. S.; Howard, B. J. *J. Mol. Spectrosc.* **1992**, *153*, 486.
(14) Bemish, R. J.; Block, P. A.; Pedersen, L. G.; Yang, W.; Miller, R. E. *J. Chem. Phys.* **1993**, *99*, 8585.
(15) Hutson, J. M.; Thornley, M. *Chem. Phys. Lett.* **1992**, *198*, 1.
(16) Yang, M.; Watts, R. O. *J. Chem. Phys.* **1994**, *100*, 3582.
(17) Yang, M.; Watts, R. O. *J. Chem. Phys.* **1994**, *101*, 8784.
(18) Bone, R. G. A. *J. Phys. Chem.* **1994**, *98*, 3126.
(19) Tao, F.; Drucker, S.; Klemperer, W. *J. Chem. Phys.* **1995**, *102*, 7289.
(20) Yang, M.; Alexander, M. H.; Werner, H.; Bemish, R. J. *J. Chem. Phys.* **1996**, *105*, 10462.
(21) Aquilanti, V.; Ascenzi, D.; Braca, E.; Cappelletti, D.; Pirani, F. *Phys. Chem. Chem. Phys* **2000**, *2*, 4081.
(22) Aquilanti, V.; Ascenzi, D.; Cappelletti, D.; de Castro Vítores, M.; Pirani, F. *J. Chem. Phys* **1998**, *109*, 3898.
(23) Cappelletti, D.; Bartolomei, M.; Pirani, F.; Aquilanti, V. *J. Phys. Chem.* **2002**, *106*, 10764.
(24) Aquilanti, V.; Ascenzi, D.; Bartolomei, M.; Cappelletti, D.; Cavalli, S.; de Castro Vítores, M.; Pirani, F. *J. Am. Chem. Soc.* **1999**, *121*, 10794.
(25) Pirani, F.; Albertí, M.; Castro, A.; Moix Teixidor, M.; Cappelletti, D. *Chem. Phys. Lett.* **2004**, *394*, 37.
(26) Cambi, R.; Cappelletti, D.; Pirani, F.; Liuti, G. *J. Chem. Phys.* **1991**, *95*, 1852.
(27) Pirani, F.; Cappelletti, D.; Liuti, G. *Chem. Phys. Lett.* **2001**, *350*, 286.
(28) Nenner, T.; Tien, H.; Fenn, J. B. *J. Chem. Phys.* **1975**, *63*, 5439; Pirani, F.; Vecchiocattivi, F. *J. Chem. Phys.* **1977**, *66*, 372.
(29) Aquilanti, V.; Ascenzi, D.; Cappelletti, D.; Pirani, F. *Nature* **1994**, *371*, 399.
(30) Aquilanti, V.; Bartolomei, M.; Cappelletti, D.; Pirani, F.; Vecchiocattivi, F.; Shimizu, Y.; Kasai, T. *Phys. Chem. Chem. Phys.* **2005**, *7*, 291.

(31) Lepère, M.; Blanquet, G.; Walrand, J.; Bouanich, J.-P. *J. Mol. Spectrosc.* **1996**, *180*, 218.
(32) Schmidt, C.; Populaire, J.-C.; Walrand, J.; Blanquet, G.; Bouanich, J.-P. *J. Mol. Spectrosc.* **1993**, *158*, 423.
(33) Hillman, J. J.; Jennings, D. E.; Hasley, G. W.; Nadler, S.; Blass, W. E. *J. Mol. Spectrosc.* **1991**, *146*, 389.
(34) Rautian, S. G.; Sobelman, I. I. *Sov. Phys. Usp.* **1967**, *9*, 701.
(35) Lance, B.; Blanquet, G.; Walrand, J.; Bouanich, J.-P. *J. Mol. Spectrosc.* **1997**, *l185*, 262.
(36) Alberti, M.; Castro, A.; Lagana, A.; Moix, M.; Pirani, F.; Cappelletti, D.; Liuti, G. *J. Phys. Chem. A* **2005**, *109*, 2906.
(37) Bernstein, R. B.; O'Brien, T. J. P. *Discuss. Faraday Soc.* **1965**, *40*, 35.
(38) Pirani, F.; Vecchiocattivi, F. *Mol. Phys.* **1982**, *45*, 1003.
(39) Pirani, F.; Vecchiocattivi, F.; van den Biesen, J. J. H.; van den Meijdenberg, C. J. N. *J. Chem. Phys.* **1981**, *75*, 1042.
(40) Aquilanti, V.; Beneventi, L.; Grossi, G.; Vecchiocattivi, F. *J. Chem. Phys.* **1988**, *89*, 751.
(41) Aquilanti, V.; Ascenzi, D.; Cappelletti, D.; DeCastro, M.; Pirani, F. *J. Chem. Phys.* **1998**, *109*, 3898.
(42) Hutson, J. M.; Green, S. *MOLSCAT: Collaborative Computational Project 6 of the UK Science and Engineering Research Council*, version 14; Daresbury Laboratory: Daresbury, UK, 1995.
(43) Baranger, M. *Phys. Rev.* **1958**, *111*, 481, 494; **1958**, *112*, 855.
(44) Fano, U. *Phys. Rev.* **1963**, *131*, 259.
(45) Ben-Reuven, A. *Phys. Rev.* **1966**, *141*, 34−40; **1966**, *145*, 7.
(46) Alexander, M. H.; Manolopoulos, D. E. *J. Chem. Phys.* **1987**, *86*, 2044.
(47) Thibault, F.; Calil, B.; Buldyreva, J.; Chrysos, M.; Hartmann, J.-M.; Bouanich, J.-P. *Phys. Chem. Chem. Phys.* **2001**, *3*, 3924.
(48) Korona, T.; Moszynski, R.; Thibault, F.; Launay, J.-M.; Bussery-Honvault, B.; Boissoles, J.; Wormer, P. E. S. *J. Chem. Phys.* **2001**, *115*, 3074.
(49) Thibault, F.; Martinez, R. Z.; Domenech, J. L.; Bermejo, D.; Bouanich, J.-P. *J. Chem. Phys.* **2002**, *117*, 2523.
(50) Domenech, J. L.; Thibault, F.; Bermejo, D.; Bouanich, J.-P. *J. Mol. Spectrosc.* **2004**, *225*, 48.
(51) Martinez, R. Z.; Domenech, J. L.; Bermejo, D.; Thibault, F.; Bouanich, J.-P.; Boulet, C. *J. Chem. Phys.* **2003**, *119*, 10563.
(52) Pack, R. T. *J. Chem. Phys.* **1983**, *78*, 7217.